Simulating Arbitrary Dose Levels and Independent Noise Image Pairs from a Single CT Scan

Sen Wang[a], Adam S. Wang[a,b]
[a]Department of Radiology, Stanford University, Stanford, CA USA 94305
[b]Department of Electrical Engineering, Stanford University, Stanford, CA USA 94305

ABSTRACT

Deep learning-based image denoising and reconstruction methods have shown promising results for low-dose CT. When high-quality reference images are not available for training the network, researchers found a powerful and effective counterpart called Noise2Noise, which trains the neural network using paired data with independent noise. However, it is uncommon to have paired CT scans with independent noise (e.g., from two scans). In this paper, a method is proposed to generate such paired data for potential usage in deep learning training by simultaneously simulating a low-dose image at arbitrary dose level and an image with independent noise from a single CT scan. Their independence is investigated both analytically and numerically. In our numerical study, a Shepp-Logan phantom was utilized in MATLAB to generate the ground-truth, normal-dose, and low-dose images for reference. Noise images were obtained for analysis by subtracting the ground-truth from the noisy images, including the normal-dose/low-dose images and the paired products of our proposed method. Our numerical study matches the analytical results very well, showing that the paired images are not correlated. Under an additional assumption that they form a bivariate normal distribution, they are also independent. The proposed method can produce a series of paired images at arbitrary dose level given one CT scan, which provides a powerful new method to enrich the diversity of low-dose data for deep learning.

Keywords: low-dose CT, synthetic CT, neural network

1. INTRODUCTION

Low-dose computed tomography (CT) is one of the most direct and effective ways to reduce the radiation dose to patients. However, a trade-off between image quality and patient dose always exists. Many efforts have been put into this area to find better ways of balancing the trade-off. Deep learning methods are one of the most recent and promising developments in reducing noise in CT imaging. When high-quality images are accessible for training, neural networks trained either in image domain[1,2] or during the reconstruction process[3,4] showed promising performance.

On the other hand, there are several works attempting to tackle the problem without the presence of high-quality images by exploiting the Noise2Noise pipeline[5]. Wu et al[6] showed that a denoising network with Noise2Noise training is equivalent to training with clean labels (high-quality images) when a few conditions are satisfied. One of the four conditions is that the network should have paired noisy data with zero-mean, independent noise. For Noise2Noise application in CT imaging, it is crucial to find such paired data. While such data could be acquired with two scans of the same patient, this exposes the patient to additional dose and will have misregistration artifacts. Pairing simulated low-dose images with the original normal-dose images does not satisfy this condition since some of the noise in the simulated low-dose image comes from the normal-dose image, so the two images do not have independent noise. In one Noise2Noise approach, Wu et al[7] constructed the independent image pairs via random projection splitting. Yuan et al[8] proposed a Noise2Noise based denoising method named 'Half2Half'. In their training pair construction, binomial selection was applied to the projection data, splitting it into two pseudo half-dose scans.

For the aforementioned methods, the dose allocation is fixed, and both of them split dose evenly to the paired images. In this paper, we propose a method to simulate arbitrary dose levels and independent noise from an existing CT scan. Paired images can be generated at any desired dose reduction level from a single CT scan, which provides more diversity in training data given the same normal-dose CT scans.

7th International Conference on Image Formation in X-Ray Computed Tomography,
edited by Joseph Webster Stayman, Proc. of SPIE Vol. 12304, 1230423
 · 0277-786X · doi: 10.1117/12.2646411

2. METHODS

For simplicity, the normal-dose projection domain measurements (raw data) P_{ND} can be modeled as the sum of a Poisson and Gaussian random variable[8]:

$$P_{ND} \sim \text{Poisson}(\lambda) + \text{Gaussian}(0, \sigma_e^2), \tag{1}$$

where λ is the mean counts and σ_e is the standard deviation of electronic noise. If we denote the photon counts from the source as I_0 and the object pathlength as l, the mean counts can be formulated as

$$\lambda = I_0 \exp(-l). \tag{2}$$

Hence, the expectation and variance of P_{ND} can be given by equations (3) and (4):

$$E[P_{ND}] = \lambda, \tag{3}$$

$$\text{Var}(P_{ND}) = \lambda + \sigma_e^2. \tag{4}$$

For a specified dose level d $(0 < d < 1)$, according to equation (1) the measured counts $P_{LD}^{(d)} \sim \text{Poisson}(d\lambda) + \text{Gaussian}(0, \sigma_e^2)$. Similarly, the expectation and variance of $P_{LD}^{(d)}$ are $E\left[P_{LD}^{(d)}\right] = d\lambda$ and $\text{Var}\left(P_{LD}^{(d)}\right) = d\lambda + \sigma_e^2$, respectively.

For the low-dose simulation process, we want to emulate the behavior of $P_{LD}^{(d)}$ at dose level *d* from normal-dose scan P_{ND}. For conventional low-dose simulation, this is a well-known process to insert noise in the projection data. Detailed steps are listed in Table 1.

Table 1. Conventional noise insertion

Step	**Operation**
1	Generate $Q \sim \text{Gaussian}(0, \lambda)$ and $E \sim \text{Gaussian}(0, \sigma_e^2)$.
2	Let $P_{sLD}^{(d)} = d\left(P_{ND} + a(Q + bE)\right)$, where $a = \sqrt{\frac{1}{d} - 1}$, $b = \sqrt{\frac{1}{d} + 1}$. Then $E\left[P_{sLD}^{(d)}\right] = d\lambda$, $\text{Var}(P_{sLD}^{(d)}) = d^2\left((\lambda + \sigma_e^2) + a^2(\lambda + b^2\sigma_e^2)\right) = d\lambda + \sigma_e^2$.
3	$P_{LD}^{(d)}$ and $P_{sLD}^{(d)}$ are independent and identically distributed random variables.

The conventional noise insertion adds additional quantum noise Q and electronic noise E, which are scaled by a factor depending on the dose level. In practice, when generating Q, we use P_{ND} as a surrogate for variance λ since the true λ is unknown from a single realization. The result is defined as:

$$P_{sLD}^{(d)} = d\left(P_{ND} + a(Q + bE)\right), \tag{5}$$

which can be viewed as a synthetic projection acquired at dose level *d* as it shares the identical probability distribution (noise properties) as $P_{LD}^{(d)}$. While this enables a simulated low-dose image, we still need a paired zero-mean, independent noise realization for Noise2Noise training. To this end, we define $P_{IN}^{(d)}$ as:

$$P_{IN}^{(d)} = d\left(P_{ND} - \frac{1}{a}\left(Q + \frac{1}{b}E\right)\right). \tag{6}$$

As is shown in the Appendix, we prove that

$$E\left[P_{sLD}^{(d)}P_{IN}^{(d)}\right] = d^2\lambda^2 = E\left[P_{sLD}^{(d)}\right]E\left[P_{IN}^{(d)}\right]. \tag{7}$$

which means that they are uncorrelated. On the assumption that $(P_{sLD}^{(d)}, P_{IN}^{(d)})$ form a bivariate normal distribution, they are independent if they are uncorrelated. This is a reasonable assumption for any modest number of photon counts, where the Poisson distribution is approximately Gaussian, and the other noise (electronic, added noise Q, E) are all Gaussian.

Importantly, both $P_{sLD}^{(d)}$ and $P_{IN}^{(d)}$ use the same noise realizations of Q and E, but they are scaled inversely and subtracted in $P_{IN}^{(d)}$ as compared to $P_{sLD}^{(d)}$, which leads to the uncorrelated property.

We thus have $P_{IN}^{(d)}$, which has zero-mean, independent noise of $P_{sLD}^{(d)}$. In the Noise2Noise conditions, independent noisy image pairs are required. The proposed method can generate such paired data ($P_{sLD}^{(d)}, P_{IN}^{(d)}$), where $P_{sLD}^{(d)}$ simulates data acquired at arbitrary dose level d. Note that $P_{IN}^{(d)}$ does not correspond to any specific dose level, but rather is designed to satisfy the Noise2Noise conditions. This enables a diversity of dose levels, which may be beneficial to training CT denoising networks.

3. NUMERICAL SIMULATION

To validate the proposed method, numerical simulation was carried out in MATLAB with the built-in Shepp-Logan phantom and Radon projection method for a monoenergetic source.

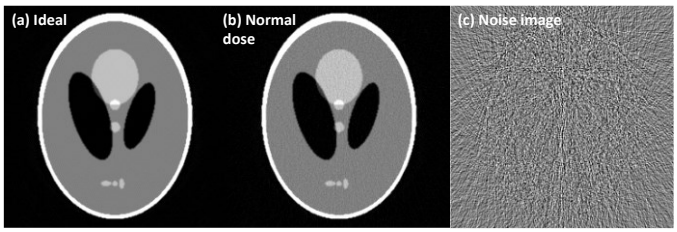

Fig. 1. Reconstructed image and noise image of Shepp-Logan phantom. (a) ideal image, noiseless ground-truth. (b) reconstructed image using normal dose, flux of source I_0= 5e4 photons, σ_e= 5 counts. (c) noise image, subtracting (a) from (b). The display window for (a) and (b) is [0, 0.4] cm^{-1}. The display window for (c) is [-0.02, 0.02] cm^{-1}.

In the simulation, the x-ray source flux was set to 5e4 photons per ray and σ_e= 5 counts, which is referred to as normal dose for the remainder of the paper.

The projections were reconstructed with filtered backprojection (FBP), and the images are illustrated in Fig. 1. We include the ideal image with noiseless projections [using equation (2)] in Fig. 1(a), which is the ground-truth image. Fig. 1(b) is the reconstructed image under normal dose [using equation (1)]. By subtracting Fig. 1(a) from Fig. 1(b), we obtain the noise image as shown in Fig. 1(c).

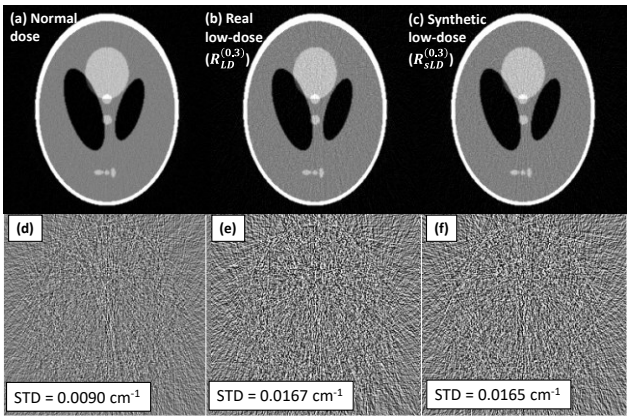

Fig. 2. Noise insertion results. (a), (b) and (c) are reconstructed and noise images for normal dose, real low-dose, and synthetic low-dose, respectively. Noise images are determined by subtracting the ground-truth image in Fig. 1(a). The display window for the first row (a-c) is [0, 0.4] cm^{-1} and is [-0.02, 0.02] cm^{-1} for the second row (d-f).

From the normal dose projections, it is possible to synthesize projections at a specific dose level following the conventional noise insertion steps in Table 1. We can also simulate a real low-dose scan acquired at the same dose level. Fig. 2 displays the results of both reconstructed and noise images for normal dose, real low-dose ($R_{LD}^{(0.3)}$, the reconstructed

image from $P_{LD}^{(0.3)}$), and synthetic low-dose ($R_{sLD}^{(0.3)}$, the reconstructed image from $P_{sLD}^{(0.3)}$), respectively, for dose level d=0.3, or 30% of the normal dose. Standard deviations of the phantom region are labeled on the noise images, where we find good correspondence between the synthetic low-dose image and the real low-dose image, as well as the increased noise in the low-dose images compared with the normal dose.

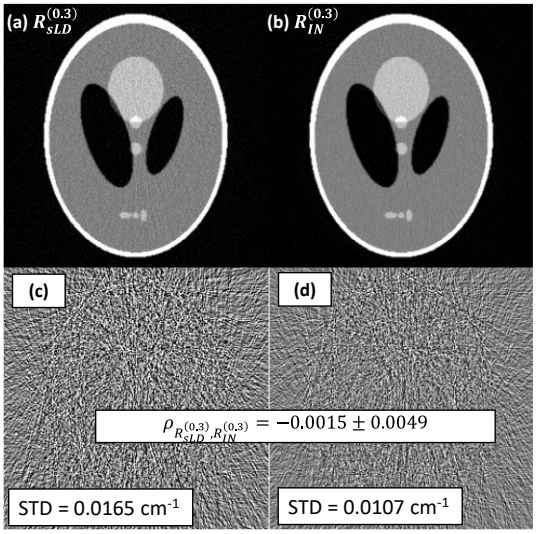

Fig. 3. Independent noise images at 30% dose level. Image $R_{sLD}^{(0.3)}$ is at simulated low dose d=0.3, and $R_{IN}^{(0.3)}$ has noise that is independent of $R_{sLD}^{(0.3)}$ ($\rho_{R_{sLD}^{(0.3)},R_{IN}^{(0.3)}} = -0.0015$), although it has a different noise magnitude. The display window is [0, 0.4] cm^{-1} for the first row and [-0.02, 0.02] cm^{-1} for the second row.

Equations (5) and (6) guide us in the generation of independent noise images from normal dose images. Fig. 3 shows a realization of the ($R_{sLD}^{(0.3)}$, $R_{IN}^{(0.3)}$) pair at 30% dose level. Correlation $\rho_{R_{sLD}^{(0.3)},R_{IN}^{(0.3)}}$ between the noise images of $R_{sLD}^{(0.3)}$ and $R_{IN}^{(0.3)}$ was calculated across all pixels in the phantom and across 10 realizations and was found to be near zero, which supports the independence we desire. As expected when $d < 0.5$, the noise magnitude in $R_{IN}^{(d)}$ is lower than that in $R_{sLD}^{(d)}$ since more noise is added into $R_{sLD}^{(d)}$ than is added to $R_{IN}^{(d)}$ according to the inverse scaling of the added quantum and electronic noise.

For other dose levels, the processing can be easily repeated, which forms the curves in Fig. 4. The horizontal axis denotes the relative dose levels from 5% to 95% of normal dose. The vertical axis is the noise in image domain. The blue squares are the real low-dose images $R_{LD}^{(d)}$ at corresponding dose levels. The red dots are noise levels of synthetic low-dose images $R_{sLD}^{(d)}$ from the normal dose image R_{ND}. Again, they fit the blue squares very well at all dose levels. The orange dots are noise levels of images $R_{IN}^{(d)}$ with independent noise from the synthetic low-dose images $R_{sLD}^{(d)}$. At lower dose, the independent $R_{IN}^{(d)}$ image tends to have lower noise level, showing different noise behaviors to real or synthetic low-dose images.

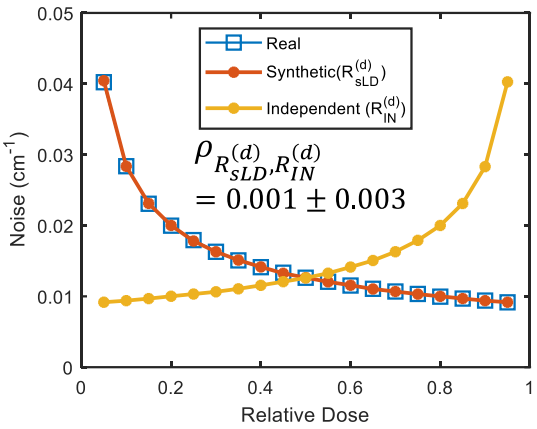

Fig. 4. Noise at different dose levels. The average correlation between images $R_{sLD}^{(d)}$ and $R_{IN}^{(d)}$ across all dose levels is $\rho_{R_{sLD}^{(d)},R_{IN}^{(d)}} = 0.001$.

In general, the independent noise image $R_{IN}^{(d)}$ does not correspond to a specific dose level, even though the noise levels appear approximately symmetric to that of the low-dose images about $d = 0.5$. For example, the noise level in $R_{IN}^{(d)}$ at 80% dose level is generally not equal to that in $R_{sLD}^{(d)}$ at 20%. However, for the special case of no electronic noise ($\sigma_e = 0$), it can be shown that this is the case, and the $R_{IN}^{(d)}$ image represents a dose level of $1 - d$.

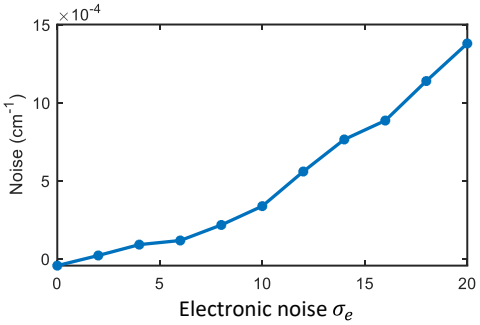

Fig. 5. Noise level difference between $R_{sLD}^{(0.5)}$ and $R_{IN}^{(0.5)}$ at 50% dose level

We demonstrate this assertion with a simple test. For the 50% dose level, we plot the difference in noise between the $R_{sLD}^{(0.5)}$ and $R_{IN}^{(0.5)}$ images (Fig. 5). When there is no electronic noise ($\sigma_e = 0$), the noise levels are indeed identical, but for $\sigma_e > 0$, more electronic noise is added to the synthetic 50% dose image $R_{sLD}^{(0.5)}$ than the independent noise image $R_{IN}^{(0.5)}$. Therefore, in general we are not splitting dose or creating another low-dose image. Instead, we have created an additional image with independent noise, which satisfies the Noise2Noise conditions.

In Fig. 6, the correlations between ($R_{sLD}^{(d)}$, $R_{IN}^{(d)}$) and ($R_{sLD}^{(d)}$, R_{ND}) are plotted in blue and red. As expected, the correlations between ($R_{sLD}^{(d)}$, $R_{IN}^{(d)}$) at different dose levels are close to 0. On the contrary, the correlations between ($R_{sLD}^{(d)}$, R_{ND}) increases with higher dose (red curve) since more of the noise in the synthetic low-dose image comes from the original normal-dose image. At lower dose, the increased amount of inserted noise leads to lower correlations with the original image.

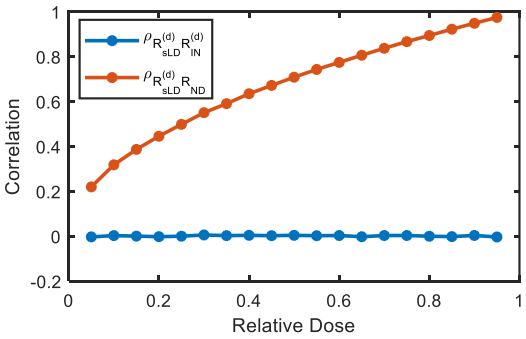

Fig. 6. Correlation at different relative dose levels

We also list the correlation coefficients under different electronic noise (σ_e) levels in Table 2. The correlation between synthetic image $R_{sLD}^{(d)}$ and independent noise image $R_{IN}^{(d)}$ is generally near zero, which agrees with the theoretical analysis in equation (7).

Table 2. Correlation coefficients

σ_e	$\rho_{R_{sLD}^{(d)},R_{IN}^{(d)}}$	
	Mean	**STD**
0	0.0003	0.0023
5	0.0011	0.0022
10	0.0014	0.0023
20	0.0008	0.0028

4. DISCUSSION AND CONCLUSIONS

In this paper, a simulation tool was demonstrated for simultaneously synthesizing low-dose images at arbitrary dose level and independent noisy images. The method extends the conventional noise insertion procedure and creates a byproduct image with independent noise along with the low-dose image at a specific dose level. Correlation between the synthetic and independent noise images was investigated both analytically and numerically, which verified that they are uncorrelated. Thus, they are independent under the assumption that they form a bivariate normal distribution.

For now, we only carried out preliminary validation with a simple simulation in MATLAB. Future work will extend these concepts to a more accurate forward projection model with polychromatic spectrum and non-ideal detector response (energy integrating or photon counting). Also, we are using a linear FBP reconstruction algorithm so that projection domain analysis can be transferred directly to the image domain (although this does include a non-linear log step). Iterative reconstruction methods may violate our linearity assumptions in the image domain, even if the projection domain noise properties hold. Another challenge might be the accuracy of our noise models in severely attenuated areas with photon starvation, such as behind metal. Lastly, we plan to demonstrate the utility of our independent noise simulation on CT denoising networks by fully leveraging the Noise2Noise principle. Our belief is that training with a wide range of simulated dose levels paired with independent noise will outperform other training methods like Half2Half or pairing simulated low dose images with normal dose images.

APPENDIX

In this section, we prove that ($P_{sLD}^{(d)}$, $P_{IN}^{(d)}$) are uncorrelated ($E\left[P_{sLD}^{(d)}P_{IN}^{(d)}\right] = E\left[P_{sLD}^{(d)}\right]E\left[P_{IN}^{(d)}\right]$). Given the definitions of $P_{sLD}^{(d)}$ and $P_{IN}^{(d)}$, it is straightforward to show

$$E\left[P_{sLD}^{(d)}\right]E\left[P_{IN}^{(d)}\right] = (d\lambda)(d\lambda) = d^2\lambda^2. \tag{8}$$

On the other side:

$$\begin{aligned} E\left[P_{sLD}^{(d)}P_{IN}^{(d)}\right] &= d^2E[P_{ND}^2 + P_{ND}\cdot a(Q+bE) - P_{ND}\cdot\frac{1}{a}\left(Q+\frac{1}{b}E\right) \\ &\quad -(Q+bE)\left(Q+\frac{1}{b}E\right)] \\ &= d^2\left(E\left[P_{ND}^2\right] - E\left[Q^2\right] - E\left[E^2\right]\right) \\ &= d^2\left(\mathrm{Var}(P_{ND}) + E^2\left[P_{ND}\right] - E\left[Q^2\right] - E\left[E^2\right]\right) \\ &= d^2\left(\lambda + \sigma_e^2 + \lambda^2 - \lambda - \sigma_e^2\right) \\ &= d^2\lambda^2 = E\left[P_{sLD}^{(d)}\right]E\left[P_{IN}^{(d)}\right] \end{aligned} \tag{9}$$

where the independence of added noise Q and E from the measured data P_{ND} gives us $E[P_{ND}Q] = 0, E[P_{ND}E] = 0$.

REFERENCES

[1] Chen H, Zhang Y, Kalra MK, et al. Low-dose CT with a residual encoder-decoder convolutional neural network. IEEE Trans Med Imaging. 2017;36(12):2524-2535.

[2] Kang E, Min J, Ye JC. A deep convolutional neural network using directional wavelets for low-dose X-ray CT reconstruction. Med Phys. 2017;44(10):e360-e375.

[3] Chun IY, Huang Z, Lim H, Fessler J. Momentum-Net: Fast and convergent iterative neural network for inverse problems. IEEE Trans Pattern Anal Mach Intell. Published online 2020.

[4] Wu D, Kim K, El Fakhri G, Li Q. Iterative low-dose CT reconstruction with priors trained by artificial neural network. IEEE Trans Med Imaging. 2017;36(12):2479-2486.

[5] Lehtinen J, Munkberg J, Hasselgren J, et al. Noise2noise: Learning image restoration without clean data. ArXiv Prepr ArXiv180304189. Published online 2018.

[6] Wu D, Gong K, Kim K, Li X, Li Q. Consensus neural network for medical imaging denoising with only noisy training samples. In: International Conference on Medical Image Computing and Computer-Assisted Intervention. Springer; 2019:741-749.

[7] Wu D, Kim K, Li Q. Low-dose CT reconstruction with Noise2Noise network and testing-time fine-tuning. Med Phys. 2021;48(12):7657-7672.

[8] Yuan N, Zhou J, Qi J. Half2Half: deep neural network based CT image denoising without independent reference data. Phys Med Biol. 2020;65(21):215020.